In-Service Diagnostics for Wire-Bond Lift-off and Solder Fatigue of Power Semiconductor Packages

Mohd. Amir Eleffendi and C. Mark Johnson, *Member, IEEE*

***Abstract*—Wire-bond lift-off and Solder fatigue are degradation mechanisms that dominate the lifetime of power semiconductor packages. Although their lifetime is commonly estimated at the design stage, based on mission profiles and physics-of-failure models, there are many uncertainties associated with such lifetime estimates, emerging, e.g., from model calibration errors, manufacturing tolerances, etc. These uncertainties, combined with the diverse working environments of power semiconductor packages result in inaccurate lifetime estimates. This paper presents an approach for estimating the extent of degradation in power semiconductor packages based on online monitoring of key parameters of the semiconductor, namely, the thermal resistance R_{thja} and the electrical resistance R_{CE}. Using these two parameters, solder fatigue and wire-bond lift-off can be detected during normal converter operation. In order to estimate these two parameters, two techniques are introduced: a residual obtained from a Kalman filter, which estimates the change in the thermal resistance R_{thja}, and a recursive least squares algorithm, which is used to estimate the electrical resistance. Both methods are implemented online and validated experimentally.**

***Index Terms*—Insulated Gate Bipolar Transistor (IGBT), kalman filtering, least squares methods, life estimation reliability, monitoring.**

I. Introduction

IGBT power modules have been reported as one of the most delicate components in power applications such as wind turbines and rail traction [1] where unpredicted failures, resulting from gradual degradation of the semiconductor packaging, can have large economic implications [2]. To help reduce the incidence of unexpected failures through condition-based maintenance (CBM), the application of online monitoring and health management algorithms has been proposed by many researchers. They aim to reduce the need for periodic maintenance and reduce system down time through continuous monitoring of key operating parameters, such as on-state voltage $V_{\mathrm{CE(ON)}}$ and junction temperature T_J, that are correlated to power module degradation. This can consequently enable predictive maintenance through the assessment of the current level of degradation of the power module.

Manuscript received August 8, 2016; revised September 26, 2016; accepted October 28, 2016. Date of publication January 26, 2016; date of current version April 24, 2017. Recommended for publication by Associate Editor T. M. Lebey.

The authors are with the Electrical and Electronics Engineering Department, University of Nottingham, Nottingham NG7 2RD, U.K. (e-mail: amir.eleffendi@eng.ox.ac.uk; Mark.Johnson@nottingham.ac.uk).

Color versions of one or more of the figures in this paper are available online at http://ieeexplore.ieee.org.

Digital Object Identifier 10.1109/TPEL.2016.2628705

Unlike lifetime estimation methods, the primary purpose of health/condition monitoring methods is to ensure protection and safe operation of power converters in their work environment rather than provide a lifetime estimate of the monitored component. The features of module degradation are extracted from the online measurements of the key failure indicators by eliminating the effects of loading and operating conditions.

As an example of health monitoring algorithm for power modules, Dawei *et al.* [3] proposed a method to detect solder fatigue, based on thermal and power loss models, to estimate the resulting change in the thermal resistance. The change in the thermal resistance was estimated by comparing an online estimate of the power loss to the original fixed power loss model. In another work, Dawei *et al.* [4] demonstrated the use of the converter output harmonics in order to detect the degradation of solder layers where the amplitude of the harmonics was correlated to the temperature and therefore the change in temperature due to solder fatigue can be detected.

Anderson and Cox [5] used principal component analysis to detect solder fatigue in IGBT modules. In this method, the on-state voltage $V_{\mathrm{CE(ON)}}$, the current I_C and the case temperature T_C are monitored and used to extract a vector of features. These extracted features are then compared with predetermined healthy features which indicate the level of degradation of solder layers from the original state.

Lehmann *et al.* [6] proposed a hardware method for the detection of wire-bond lift-offs during normal operation of power modules by adding sensing wires in the packaging which are bonded to the emitter contact on the chip. At the moment when wire-bonds fail, changes in the voltage difference across these sensing wires indicates a wire-bond failure. A resistor is used to increase the impedance of the current path, preventing high current from flowing through the sense wires.

The online measurement of key failure indicators (e.g., junction temperature and on-state voltage) has been identified as a limiting factor for the development of efficient PHM for power electronics [7] and consequently, much recent research has been dedicated to propose online measurement circuits of failure indicators and thermo-sensitive electrical parameters [8]–[11]. However, little has been done in terms of using these online measurements to extract health information about the state of wire-bonds and solder layers of IGBT modules.

This paper focuses on the use of the online measurements of on-state voltage $V_{\mathrm{CE(ON)}}$ and online estimate of junction temperature T_J to monitor the degradation in power semiconductor modules resulting from wire-bonds lift-off and solder fatigue.

Fig. 1. Power cycling test equipment "Mentor Graphics Power Tester 1500 A."

Changes in key failure indicators of the power IGBT modules, namely the thermal resistance R_{thja} and electrical resistance R_{CE}, are estimated. Model-based residuals are used to detect changes in R_{thja} through the residual produced by a Kalman filter algorithm that is employed to estimate junction temperature. A recursive least squares (RLS) algorithm is used to estimate the collector–emitter resistance R_{CE}, which is shown to be correlated to wire-bond failure.

II. Effects of Package Aging on Failure Indicators

In order to investigate the effect of packaging degradation on the electrical and thermal characteristics of IGBT modules, power cycling tests were carried out using a "Mentor Graphics Power Tester 1500A" [12], which is an industrial power cycling equipment, illustrated in Fig. 1. This equipment is capable of measuring $V_{\mathrm{CE(ON)}}$ and the transient thermal impedance Z_{thja} during power cycling tests. It is well known that the on-state resistance R_{CE} and on-state voltage $V_{\mathrm{CE(ON)}}$ are correlated to wire-bond lift-offs, where step-wise changes are a feature of individual wire lift-off. Similarly changes in the transient thermal impedance can be related to progressive degradation of the thermal path resulting from solder fatigue (at die-attach and/or substrate mount-down layers) [13]. Together these features allow the state of the wire bonds as well as the state of the thermal conduction path to be monitored.

Two different power cycling tests were carried out to investigate the effects of wire-bond lift-off and solder fatigue on electrical resistance R_{CE} and thermal resistance R_{thja}.

A. *Effects of Solder Fatigue on* R_{thja}

The IGBT module subjected to cycling was an off-the-shelf half-bridge 1.2 kV/200 A module. Each switch of the half-bridge has two IGBT devices which are connected in parallel and each device is positioned on a separate substrate tile making four substrate tiles in total. However, only one switch of the half-bridge module was cycled. The cycling current I_C was fixed at 170 A, which gave an initial temperature swing at the junction $\Delta T_J = 120\,^{\circ}\mathrm{C}$ with a maximum of $T_{J\max} = 140\,^{\circ}\mathrm{C}$ and a minimum of $T_{J\min} = 20\,^{\circ}\mathrm{C}$, as estimated from the measured values of V_{CE}. The heating time and cooling time were fixed at 65 and 70 s, respectively. The test started with an initial power dissipation $P_D = 344\,\mathrm{W}$ measured at the peak temperature of 140 °C. Transient thermal impedance measurements were made at a fixed interval of 1000 cycles during the cycling. This interval was reduced to 500 cycles by the end of the test in order to get better insight of the change in thermal resistance R_{thja} in relation to the degradation.

Transient thermal impedance measurement Z_{thja} is achieved using the collector–emitter voltage V_{CE} as a thermos-sensitive electrical parameter. To achieve this measurement, the IGBT is heated using a high current source to reach thermal equilibrium, and then the high current is removed to allow the IGBT to cool down and reach thermal equilibrium again. V_{CE} is measured across the IGBT during the cooling phase at a low current of 200 mA. A calibration curve $T_J = f(V_{\mathrm{CE}})$, predetermined at that current value, is used to calculate the temperature swing ΔT_J, which is then normalized using the power dissipation to produce the thermal impedance Z_{thja}. The module under test is mounted on a water-cooled cold plate whose temperature is maintained constant at 20 °C.

In order to accelerate the degradation of the substrate to baseplate solder layer, a Kapton film of 25 μm thickness was placed between the baseplate of the module and the cold plate [13]. This increases the temperature swing at the internal solder layers compared to directly mounting the module on the cold plate, thus accelerating the rate of degradation.

Measurement of transient thermal impedance Z_{thja} were made with the module *in situ*, without disturbing the physical mounting of the module from the cold plate. A heating current of 150 A was used for the transient thermal measurement which produced a power dissipation step of 360 W. Fig. 2 shows the junction-to-ambient transient thermal impedance Z_{thja} measurements performed during the power cycling test, indicating a clear increase in Z_{thja} with the number of cycles. The thermal resistance R_{thja} is the steady-state value of Z_{thja}. Fig. 3 shows the value of R_{thja} during the power cycling test. It can be seen that R_{thja} remained almost constant until 7100 cycles and then started to increase, gradually at first and then with an increasing rate. This increment is correlated to the degradation in the thermal path, in this case as a result of solder fatigue.

In order to confirm the cause of this increment in R_{thja}, scanning acoustic microscopy (SAM) of the IGBT module was performed before and after the power cycling test. The reflected ultrasonic echoes show discontinuities in the internal layers of the module and appear as dark shadows in the images. Fig. 4

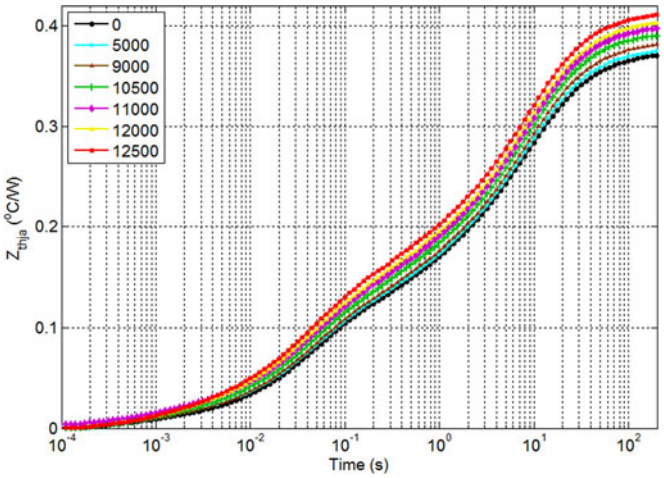

Fig. 2. Transient thermal measurement at different cycles as measured during the power cycling test.

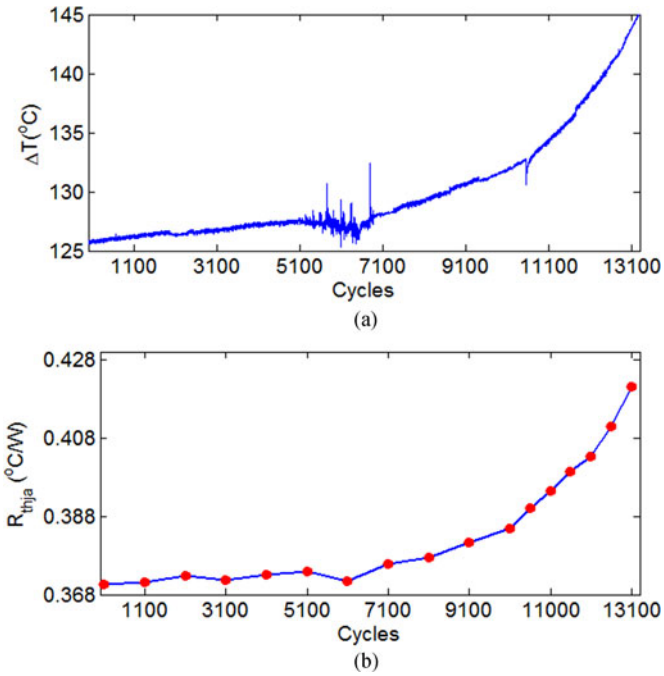

Fig. 3. Junction-to-ambient thermal resistance R_{thja} during the power cycling test.

(left) shows the SAM image of the cycled switch in the module before power cycling, whereas Fig. 4 (right) shows the SAM image of the cycled switch after 13 500 cycles. It can be seen from these images that cracking has occurred within the die-attach layer and also within the substrate mount-down solder layer. At the substrate mount-down solder layer, cracking propagates from the corners at the right-hand side of the substrate toward the center. A similar behavior can be observed at the die-attach layer where the corners appear darker than the center indicating cracking. These images confirm the correlation between the solder fatigue at die-attach and substrate mount-down solder and the change in thermal resistance R_{thja} shown earlier. An extensive study was made in [13] detailing this correlation.

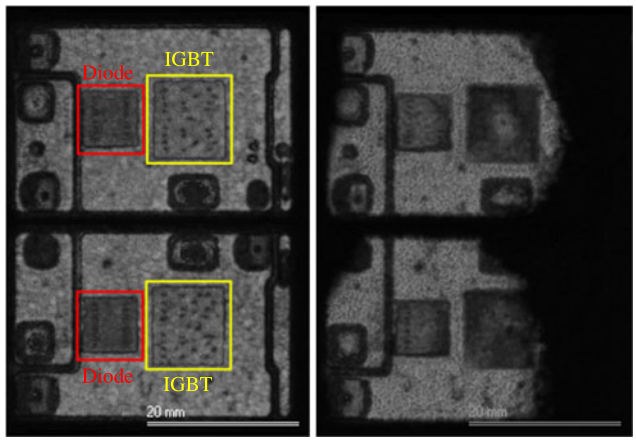

Fig. 4. SAM image of the tested IGBT power module in its original condition before cycling (Left) and after power cycling (Right).

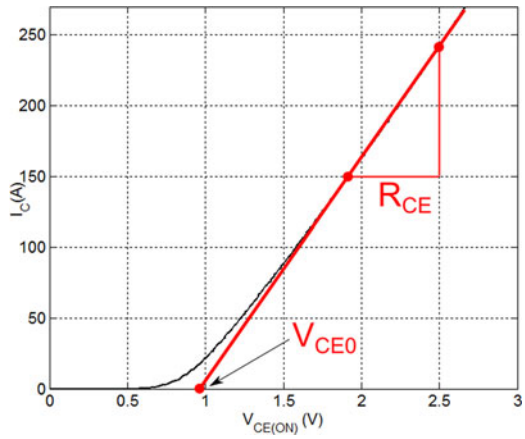

Fig. 5. Linearization of the forward characteristic of an IGBT.

B. *Effect of Wire-Bond Lift-offs on* R_{CE}

The electrical resistance R_{CE} of an IGBT can be calculated from the forward characteristic of the IGBT measured across collector and emitter terminals. This forward characteristic can be approximated by a straight line, as shown in Fig. 5, and may be described by

$$V_{\mathrm{CE}} = R_{\mathrm{CE}} I_C + V_{\mathrm{CE0}} \tag{1}$$

where $R_{\mathrm{CE}} = \Delta V_{\mathrm{CE}}/\Delta I_C$ is the slope of the line and represents the electrical resistance of the IGBT. V_{CE0} is the x-intercept of line with the current axis. This is a common approximation to simplify the modeling of the forward characteristic [14].

To investigate the effect of wire-bond degradation on the collector–emitter electrical resistance R_{CE}, six IGBT devices were subjected to power cycling. The cycled IGBT devices were connected, as shown in Fig. 6. All devices were forward biased with $V_{\mathrm{GE}} = 15$ V. The total cycling current for the IGBTs was $I_C = 270$ A, which generated a total power loss of 762 W. This resulted in a temperature swing at the junction, $\Delta T_J = 137$ °C. This temperature swing is an average across six IGBTs. Due to technical limitations, the measurement of $V_{\mathrm{CE(ON)}}$ can only

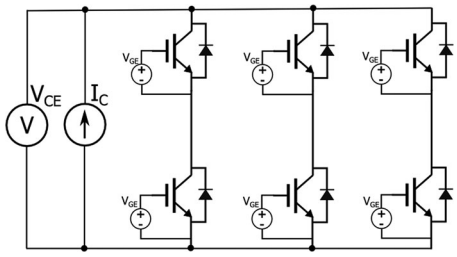

Fig. 6. Connection of tested IGBT devices on the power cycling equipment.

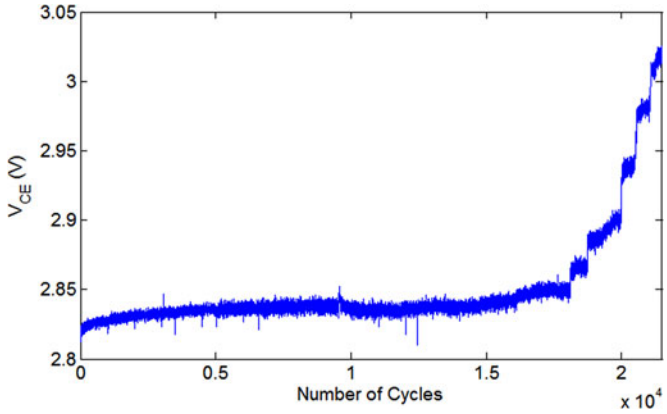

Fig. 7. On-state voltage of cycled IGBT devices equipment.

be made across the whole setup for six IGBTs. However, this limitation does not affect the outcome of the test. The power cycling test was stopped after 21 400 cycles when the value of $V_{\mathrm{CE(ON)}}$ had risen 0.2 V above its starting level. It should be noted that all devices were still functional after the test was stopped.

The on-state voltage $V_{\mathrm{CE(ON)}}$ of the IGBT devices monitored during the power cycling test is shown in Fig. 7. The voltage $V_{\mathrm{CE(ON)}}$ remained constant until about 18 150 cycles, where step-wise increments started to appear. This step-wise behavior is known to be caused by wire-bond lift-off.

The measured increase in the on-state voltage $V_{\mathrm{CE(ON)}}$ is caused by an increment of the collector–emitter circuit electrical resistance R_{CE}. This resistance R_{CE} is a summation of the electrical resistance of the semiconductor chip, the wire bonds, copper traces, and the connection terminals. However, among these different components, only the electrical resistance of the wire bonds changes due to degradation. Therefore, wire-bond lift-off will increase R_{CE} [15], which consequently increases the voltage $V_{\mathrm{CE(ON)}}$.

After the power cycling test was stopped, the forward characteristic of each individual IGBT was obtained using a curve tracer at room temperature. Fig. 8 shows the forward characteristic of each IGBT compared to the forward characteristic before cycling. The forward characteristics of all tested IGBTs were identical before cycling, therefore, only one original characteristic is shown here for clarity. The cycled IGBTs show different levels of change in the slope of their forward characteristics. The slope, as described earlier, represents the electrical resistance R_{CE}. Table I shows the parameters of (1) obtained by

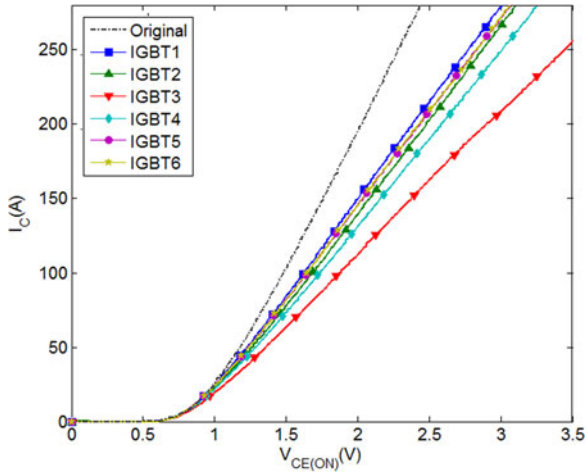

Fig. 8. Forward characteristic of cycled IGBTs compared to original characteristic before cycling.

TABLE I
CHANGE IN R_{CE} AND V_{CE0} DUE TO WIRE-BOND FAILURE

IGBT	Original	1	2	3	4	5	6
R_{CE} (mΩ)	5.315	7.747	7.868	10.56	8.461	7.991	7.906
V_{CE0} (V)	0.930	0.8377	0.9048	0.7971	0.8927	0.8362	0.8494

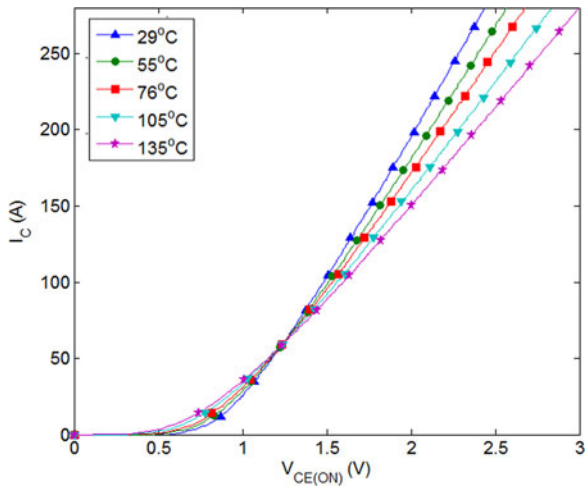

Fig. 9. Forward characteristic of a 1.2 kV/200 A IGBT module at multiple temperatures.

curve fitting to the data in Fig. 8. Compared with the original value, it can be seen that R_{CE} of IGBT3 is the highest, followed by IGBT4. The lowest R_{CE} is for IGBT1, which is the least degraded sample. The value of V_{CE0} on the other hand shows no discernible correlation with the observed changes in the forward characteristic. The different slopes (i.e., different R_{CE} values) are believed to be caused by different levels of degradation in the wire bonds of the tested IGBTs.

However, it is well known that the forward characteristic of an IGBT is a function temperature, and therefore, the parameters R_{CE} and V_{CE0} can also change with temperature. Fig. 9

TABLE II
CHANGES OF R_{CE} AND V_{CE0} WITH TEMPERATURE

T (°C)	29	55	76	105	135
R_{CE} (mΩ)	5.453	6.05	6.531	7.237	7.966
V_{CE0} (V)	0.9297	0.8965	0.8707	0.8301	0.7904

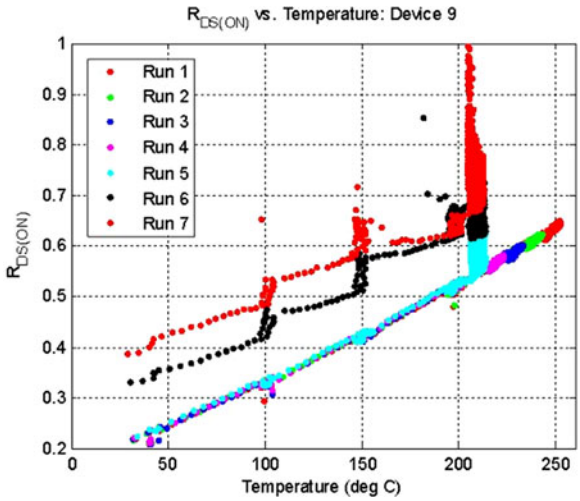

Fig. 10. Correlation between R_{CE} and temperature. Wire-bond lift-off changes the offset of the linear correlation. The slope remains constant [16].

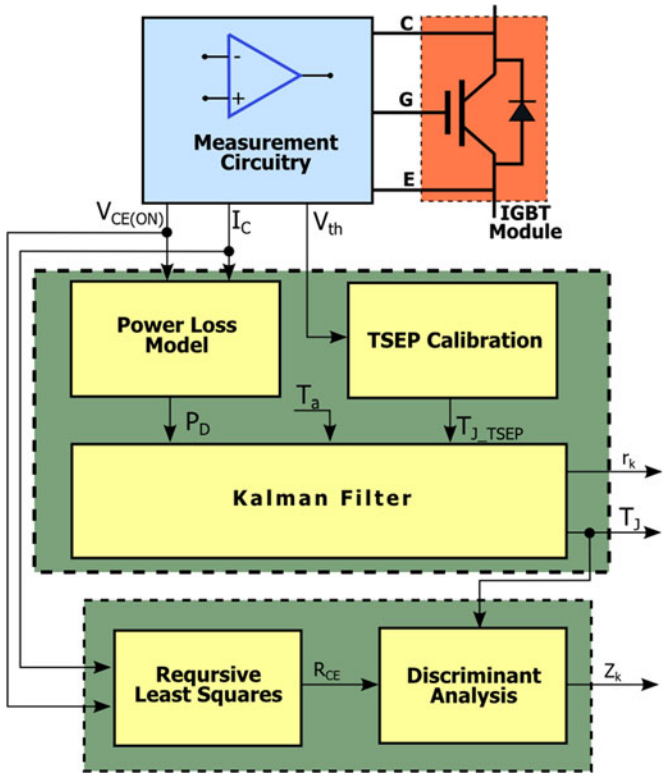

Fig. 11. Proposed method for monitoring wire-bonds lift-off and solder fatigue.

shows the forward characteristic of a pristine IGBT at multiple temperatures. The inflection point is a common feature in the forward characteristic of an IGBT device when characterized at multiple temperatures. A negative temperature coefficient influences the characteristic below the inflection point, whereas a positive temperature coefficient influences the characteristic above the inflection point.

The approximately linear relationship between current I_C and voltage $V_{\mathrm{CE(ON)}}$ is observed above the inflection point, and therefore, it is in this region that the electrical resistance R_{CE} is calculated. Note that since the majority of IGBTs will operate in this region for some of the time [14], this will not limit the application of the method of calculation. The slope R_{CE}, in this region, has a positive temperature coefficient that results in higher on-state voltage $V_{\mathrm{CE(ON)}}$ at higher temperatures at any current value. Table II shows the variation of R_{CE} and V_{CE0} with temperature for an undegraded IGBT.

From the above, it can be said that wire-bond failures and temperature both result in increases in the electrical resistance R_{CE}. However, the sensitivity of R_{CE} to temperature (rather than the absolute value) is largely determined by the physical chip structure of the semiconductor and is not, therefore, affected by wire-bond lift-off. Thus, the effect of wire-bond lift-offs appears as an offset on the function $R_{\mathrm{CE}} = f(T)$, as shown in Fig. 10. Steps appear in Fig. 10 are due to experimental setup [16].

Hence, it is necessary to consider the changes in temperature when monitoring R_{CE}, since an increment in R_{CE} can either be justified due to an increment in temperature or due to a wire-bond lift-off. A method to deal with this problem is proposed later in this paper.

III. BACKGROUND OF PROPOSED METHODS

To enable the condition monitoring of power semiconductor packaging, failure indicators of R_{CE} and R_{thja} should be monitored. However, these two parameters cannot be measured by direct methods during the normal operation of power converters and therefore, indirect methods must be utilized to obtain the values of these two parameters.

Fig. 11 shows a block diagram of the proposed method. The measurement circuits collects the current I_C, on-state voltage $V_{\mathrm{CE(ON)}}$ and gate threshold voltage $V_{\mathrm{G(th)}}$ from the power semiconductor (an IGBT in this case). The gate threshold voltage $V_{\mathrm{G(th)}}$ is a thermo-sensitive electrical parameter Thermo-Sensitive Electrical Parameters (TSEP) and it is used to calculate the junction temperature T_J of the IGBT module. Gate threshold voltage $V_{\mathrm{G(th)}}$ has a linear correlation to temperature and a relatively higher sensitivity to T_J compared to $V_{\mathrm{CE(ON)}}$. Estimation of T_J is realized using Kalman filter algorithm which requires the ambient temperature T_a and the power loss P_D as inputs. The power loss calculation is achieved using look-up tables, based on the measured current, on-state voltage and duty ratio. A full explanation of the use of a Kalman filter for junction temperature estimation can be found in another work by the authors [17]. An additional feature of using the Kalman filter is the residual signal r_k generated as part of the predict-correct sequence. The residual is the difference between the model esti-

mates of T_J and the true measurement of T_J obtained from the TSEP. Since the model is fixed, this deviation is correlated to changes in the thermal resistance R_{thja}, and therefore, it can be used to monitor the thermal degradation of the semiconductor packaging due to solder fatigue.

As for wire-bond lift-off, the RLS algorithm is used to estimate the electrical resistance R_{CE} from the online measurement of $V_{\mathrm{CE(ON)}}$ and I_C. However, as explained earlier, R_{CE} is also sensitive to temperature variations, and therefore, the effect of T_J on the estimate of R_{CE} should be eliminated. For this purpose, discriminant analysis is applied to produce a linear transformation Z_k from the estimate of R_{CE} and T_J. This linear transformation Z_k reveals the changes in R_{CE} that are caused by wire-bond lift-offs whereas the variations of T_J do not affect the value of Z_k. In this way, Z_k can be used to monitor wire-bonds lift-off.

A. Kalman Filter Residual

Residuals are defined as quantities that represent the discrepancy between measured variables and their expected values given under a healthy baseline state. The expected value is obtained from a reference model that represents the power module in its original state. Residuals can be obtained using a range of different methods [18], e.g., parity equations, diagnostic observers, and Kalman Filters. In this paper, the Kalman Filter is used as a residual generator to monitor the health state of the thermal path in an IGBT power module. And therefore, an electrical equivalent model of the thermal path is used by the Kalman Filter [17]. After the residual is calculated, it is evaluated statistically to reveal deviations in its mean value from the original mean value under health conditions. Changes in the mean value of the residual are correlated to changes in R_{thja} which, therefore, give indications of the thermal degradation due to solder fatigue.

It is well known that the heat conduction path of power semiconductor packages can be represented by an R_{C} electrical equivalent network. This R_{C} network can be expressed by the following discrete state-space representation:

$$\begin{aligned} x_k &= \boldsymbol{F} x_{k-1} + \boldsymbol{L} u_k \\ y_k &= \boldsymbol{H} x_k + \boldsymbol{J} u_k \end{aligned} \tag{2}$$

where k is the time step index, x is the state vector, u is the input vector, y is the output vector and *F, L, H,* and *J* are the system parameters that can be obtained by curve fitting of the measured thermal impedance Z_{th}. Assuming that matrices *F, L, H*, and *J* represents the thermal system in its original state, then ΔF, ΔL, ΔH, and ΔJ represents changes in the thermal system parameters resulting from solder fatigue. In addition, assuming the existence of process and measurement noise terms w_k and v_k, and a disturbance term d_k, this modified state-space model can be represented by

$$\begin{aligned} x_k &= (\boldsymbol{F} + \boldsymbol{\Delta F})\, x_{k-1} + (\boldsymbol{L} + \boldsymbol{\Delta L})\, u_k + d_k + w_k \\ y_k &= (\boldsymbol{H} + \boldsymbol{\Delta H})\, x_k + (\boldsymbol{J} + \boldsymbol{\Delta J})\, u_k + v_k. \end{aligned} \tag{3}$$

Using this state-space model, the state estimate $\hat{x}_k$ and the estimated output $\hat{y}_k$ produced by the Kalman filter are given by the following expression (assuming that the feedforward matrix $J = 0$ for simplification):

$$\hat{x}_k = \boldsymbol{F}\hat{x}_{k-1} + \boldsymbol{K}\left[y_k - \hat{y}_k\right] \tag{4}$$

$$\hat{y}_k = \boldsymbol{H}\hat{x}_{k-1} \tag{5}$$

where $\hat{\mathrm{x}}$ is the state estimate vector, $\hat{\mathrm{y}}$ is the output estimate vector, and K is the Kalman Gain matrix. Assuming that the state estimate error is e_k, which is the difference between the true state vector x and the estimated state vector $\hat{\mathrm{x}}$, and assuming that the residual r_k is the difference between the measured output y_k and the estimated output $\hat{y}_k$:

$$e_k = x_k - \hat{x}_k \tag{6}$$

$$r_k = y_k - H\hat{x}_k^-. \tag{7}$$

Using (3) and (4), the state estimation error e_k can be derived as

$$\begin{aligned} \boldsymbol{e_k} = {} & \left[(\boldsymbol{F} + \boldsymbol{\Delta F}) - \boldsymbol{K}\left(\boldsymbol{H} + \boldsymbol{\Delta H}\right)\right] \boldsymbol{e_{k-1}} \\ & + \left(\boldsymbol{L} + \boldsymbol{\Delta L}\right) \boldsymbol{u_k} + \boldsymbol{d_k} + \boldsymbol{w_k} + \boldsymbol{K v_k}. \end{aligned} \tag{8}$$

And the residual r_k can then be written in terms of e_k as

$$r_k = (\boldsymbol{H} + \boldsymbol{\Delta H})\, e_k + v_k. \tag{9}$$

This expression shows that the residual r_k is driven by the state estimation error e_k in (8). Consequently, the residual is affected by changes in the thermal system ΔF, ΔL, ΔH, which are caused by solder fatigue. The residual is also affected by the disturbances d_k, and changes in the noise terms w_k and v_k.

Therefore, in the ideal case where no modeling errors are present and no disturbances are acting on the system, the residual r_k has a mean value of zero for the original undegraded system. However, in practice these conditions may not hold since modeling errors are unavoidable and external disturbance (e.g., cooling conditions) can affect the thermal system which leads to the residual r_k having an initial nonzero value under a healthy state of the thermal path.

B. RLS Algorithm

The linear approximation of the forward characteristic shown in (1) can be used to estimate the electrical resistance R_{CE} from the online measurement of I_C and $V_{\mathrm{CE(ON)}}$. For this purpose, the RLS estimate is used. The advantages of using RLS algorithm resides in its capability to find the coefficients of a function given a set of noisy measurement recursively in time eliminating the need to store measurement data. This makes it a suitable solution for online applications. It is an adaptive algorithm that estimates coefficients by minimizing a cost function providing the ability to track ongoing changes in estimated parameters. And therefore, it is good candidate for monitoring changes in R_{CE} resulting from wire-bond lift-offs.

Suppose $(x_i,\, y_i)$ are points of a given measurement dataset $(I_C,\, V_{\mathrm{CE(ON)}})$, where $i = 1, 2, \ldots, N$ and *N* is the size of the dataset. This data $(x_i,\, y_i)$ can be assumed to be generated by a model $y_i = f(x_i)$

$$f\left(x_i\right) = a_1 g_1\left(x_i\right) + \ldots + a_m g_m\left(x_i\right) \tag{10}$$

where $g_j(x)$ is called a regressor and $(a_1, \ldots, a_m)$ are unknown model parameters. This model can be written in a matrix format as following:

$$y = \emptyset\theta \tag{11}$$

where $\emptyset = [\vartheta_1^T, \vartheta_2^T, \ldots, \vartheta_N^T]^T$, $\vartheta_i^T = [g_1(x_i),\ g_2(x_i), \ldots,\ g_m(x_i)]$, and $\theta = [a_1,\ a_2,\ \ldots,\ a_m]^T$ and superscript *T* refers to a matrix transposition. The vector θ is a vector of unknown parameters $(R_{\mathrm{CE}},\ V_{\mathrm{CE0}})$ that need to be determined from the given measurement data $(x_i,\ y_i)$. The least squares estimate of the vector θ is $\hat{\theta}$ which can be calculated by minimizing the cost function

$$V(\theta) = \frac{1}{2}\varepsilon^T\varepsilon \tag{12}$$

where $\varepsilon = [e(x_1), e(x_2), \ldots, e(x_N)]^T$ is a vector of the "Equation error" which is defined by

$$e(x_i) = y_i - f(x_i). \tag{13}$$

The cost function $V(\theta)$ has a minimum when its gradient is set to zero. The solution of the resulting problem gives the following estimate:

$$\hat{\theta} = \left(\emptyset^T\emptyset\right)^{-1}\emptyset^T Y \tag{14}$$

where $\emptyset^T\emptyset$ is a positive definite matrix and $Y = [y_1,\ y_2,\ \ldots,\ y_N]$. However, in order to enable the real-time implementation of this estimate, it should be written in a recursive form.

Assuming the time step index is *n*, then the estimate $\hat{\theta}(n)$ at a time instant *n* is determined from the estimate $\hat{\theta}(n-1)$ at the previous time step in addition to the measurement data available at *n*

$$\hat{\theta}(n) = \hat{\theta}(n-1) + K(n)\left[y(n) - \emptyset^T(n)\,\hat{\theta}(n-1)\right] \tag{15}$$

where $K(n)$ is called the gain vector and it is a weighting factor that determines the influence of the previous estimate $\hat{\theta}(n-1)$. Assuming $\varepsilon(n) = y(n) - \emptyset^T(n)\hat{\theta}(n-1)$ is the error signal, and $P(n) = (\emptyset^T(n)\emptyset(n))^{-1}$ is the covariance of the estimate $\hat{\theta}(n)$, the RLS algorithm can be stated by the following equations:

$$\hat{\theta}(n) = \hat{\theta}(n-1) + K(n)\,\varepsilon(n) \tag{16}$$

$$K(n) = \frac{P(n-1)\,\emptyset^T(n)}{\lambda + \emptyset^T(n)\,P(n-1)\,\emptyset^T(n)} \tag{17}$$

$$P(n) = \lambda^{-1}\left[P(n-1) - \frac{P(n-1)\ \emptyset(n)\ \emptyset^T(n)\,P(n-1)}{\lambda + \emptyset^T(n)\,P(n-1)\,\emptyset^T(n)}\right] \tag{18}$$

where $\lambda \leq 1$ is a forgetting factor, which can be tuned to produce the smallest estimate variance. An initialization of $\hat{\theta}(0)$ and $P(0)$ of the RLS is required. A common choice for these initial values is $\hat{\theta}(0) = 0$ and $P(0) = \delta I$, where *I* is the unity matrix and $\delta >> 1$.

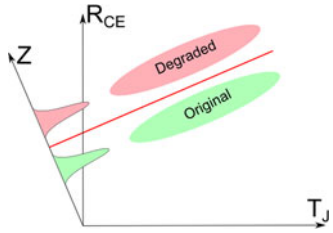

Fig. 12. Graphical explanation of the discriminant analysis method. The two dimensional data are projected on the discriminant to measure the deviation from its original value.

C. Discriminant Analysis

The value of R_{CE} estimated by the RLS algorithm is dependent on temperature T_J, and therefore, in order to detect changes in R_{CE} caused by wire-bond lift-offs, the effect of T_J has to be eliminated. To achieve this, discriminant analysis method is used.

Discriminant analysis is explained in Fig. 12. Considering two separate data groups (Original) and (Degraded), a discriminant line can be chosen to achieve the best separation between the two groups. The discriminant line can be linear or quadratic depending on the data patterns. In our case, considering the data in Fig. 10, a straight line can achieve good separation between original and degraded IGBTs. The normal distance of a data point $(T_J,\ R_{\mathrm{CE}})$ from the discriminant line is determined by a linear transformation *Z*

$$Z = a_1 R_{CE} + a_2 T_J \tag{19}$$

where the parameters a_1 and a_2 can be determined from training data such that the distance between the mean value vectors $\bar{\boldsymbol{R}}_{\boldsymbol{CE}} = [\bar{R}_{\mathrm{CEO}},\ \bar{R}_{\mathrm{CED}}]$ and $\bar{\boldsymbol{T}}_{\boldsymbol{J}} = [\bar{T}_{JO},\ \bar{T}_{JD}]$ is maximized, where $(\bar{R}_{\mathrm{CEO}},\ \bar{T}_{JO})$, and $(\bar{R}_{\mathrm{CED}},\ \bar{T}_{JD})$, represent the center of the (Original) and (Degraded) groups, respectively. a_1 and a_2 can be determined solving the equation

$$\boldsymbol{a} = \boldsymbol{S}_{pl}^{-1}\left(\bar{\boldsymbol{R}}_{\boldsymbol{CE}} - \bar{\boldsymbol{T}}_{\boldsymbol{J}}\right) \tag{20}$$

where $a = [a_1, a_2]$ and S_{pl} is the covariance matrix $\mathrm{Cov}(R_{\mathrm{CE}}, T_J)$. The linear transformation *Z* of a data point (R_{CE}, T_J) is a scalar which takes a negative value if the point (R_{CE}, T_J) is below the discriminant line, a zero value if the data point (R_{CE}, T_J) is located on the line or a positive value if it is above the line.

The discriminant line, therefore, must be chosen to be parallel to the function $R_{\mathrm{CE}} = f(T_J)$ such that any changes in R_{CE} caused by a corresponding change in T_J will not affect the normal distance *Z* as is described in Fig. 12. And therefore, *Z* is only sensitive to changes in R_{CE} that are not associated with a change in T_J, which is the case for wire-bond lift-offs.

IV. Experimental Setup

A full-bridge inverter, shown schematically in Fig. 13(a), was used as an experimental apparatus to validate the proposed method. Online measurements of the on-state voltage $V_{\mathrm{CE(ON)}}$ and gate threshold voltage $V_{\mathrm{G(th)}}$ were achieved using a purpose-designed circuit [19] during normal converter

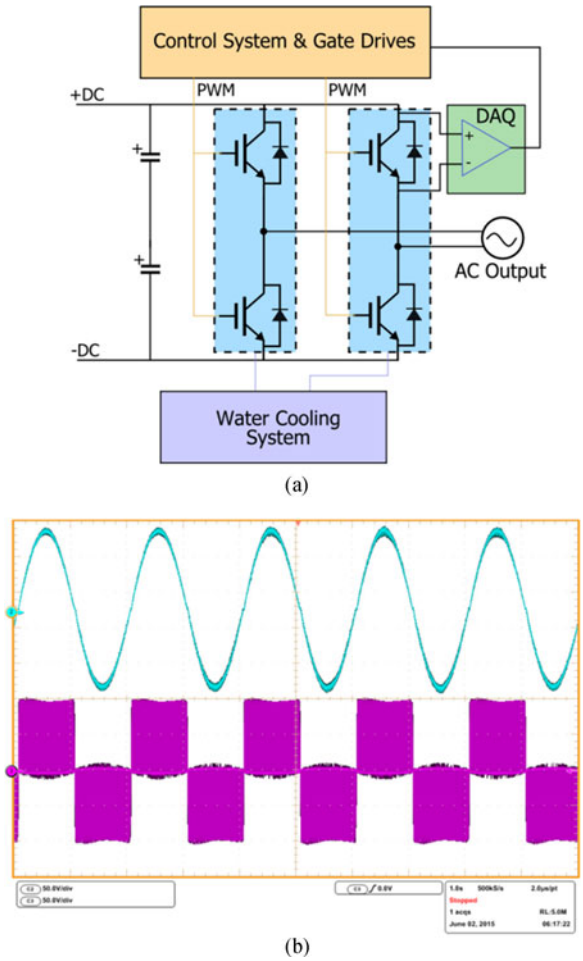

Fig. 13. (a) Block diagram of the full-bridge inverter used for validating the diagnostic method. (b) Output current and output voltage of the inverter measured using an oscilloscope.

operating conditions. The junction temperature T_J was estimated online by applying the Kalman filter algorithm to a thermal model in which the temperature "measurements" were derived from the measured gate threshold voltage $V_{\mathrm{G(th)}}$ [17]. A dSPACE system was used to collect the measurement data and to implement the condition monitoring algorithms in addition to a PI current controller which was used to control the output current of the inverter. An inductor of 300 mH was used as a load for the inverter. A controllable power supply provided the input dc voltage and water cooling was used to remove the generated heat from the modules. The switching frequency for the inverter was fixed at 1 kHz, whereas the modulation frequency and amplitude was adjustable. Typical inverter output current and voltage waveforms, as measured by an oscilloscope, are shown in Fig. 13(b). The online measurement data of the current I_C, on-state voltage $V_{\mathrm{CE(ON)}}$, and gate threshold voltage $V_{\mathrm{G(th)}}$ is shown in Fig. 14.

In order to accelerate the failure mechanisms of solder fatigue and wire-bond lift-off, the IGBT power modules were installed on the mentor graphics power cycling equipment and cycled over a junction temperature range of 20 °C to 140 °C using the power tester current source. The power cycled IGBT

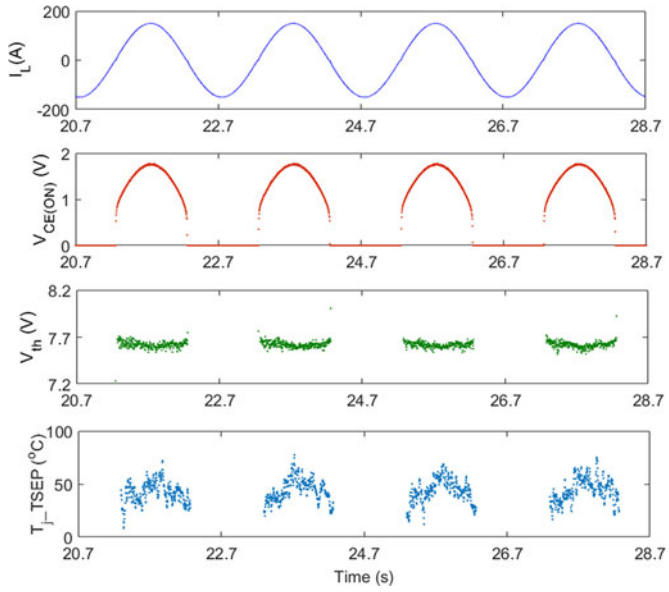

Fig. 14. Online measurement data of current I_L, $V_{\mathrm{CE(ON)}}$, $V_{\mathrm{G(th)}}$, and $T_{\mathrm{j_T\,SEP}}$ as acquired by the dSPACE system.

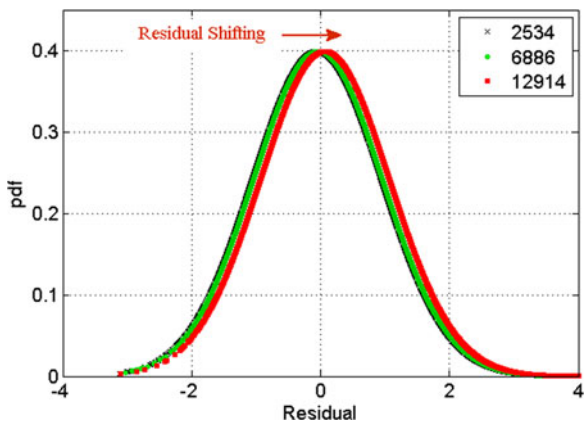

Fig. 15. Statistical distribution (pdf) of the residual changes as number of cycles progresses indicating a change in the thermal path.

modules were then reconfigured, without demounting them from the cold plate, as an inverter with the dSPACE controller, to collect the online measurement data and run the condition monitoring algorithms. This process was repeated at intervals during the power cycling tests in order to evaluate the performance of the online condition-monitoring algorithms. Note that the results of the power cycling tests, namely changes in R_{th} and R_{CE}, determined from the power tester, are those presented in Section II.

V. Results

A. Thermal Path Degradation

To monitor the degradation of the thermal path, the residual from the Kalman filter is used. The online measurement data was collected from the inverter setup at frequent intervals of the power cycling test as described in Section IV.

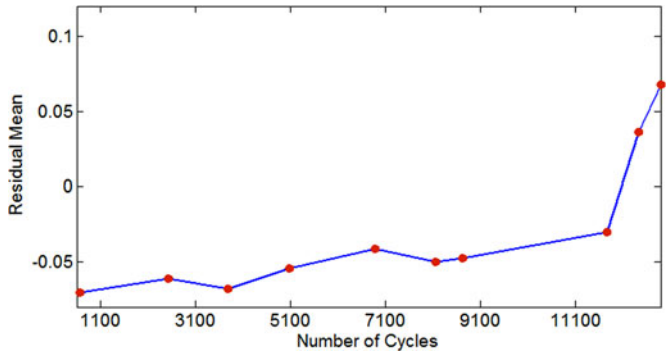

Fig. 16. Mean of the residual of T_{J} given by V_{th} as a function of number of cycles.

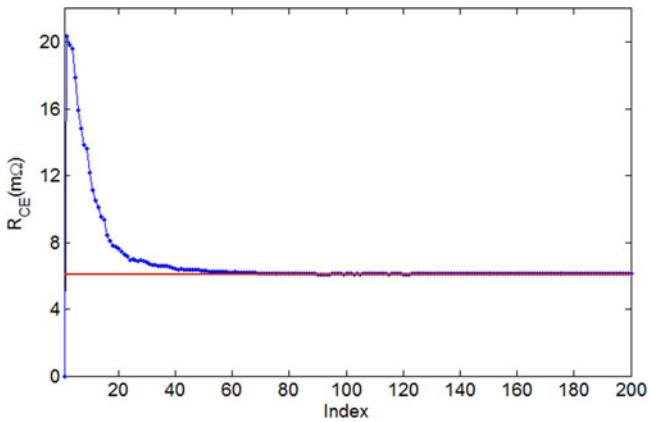

Fig. 17. Convergence of RLS algorithm to the true value of R_{CE}.

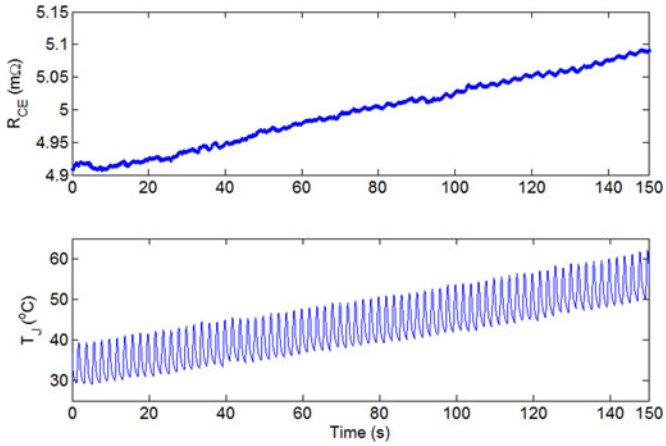

Fig. 18. Estimated R_{CE} with RLS algorithm follows the change in estimated T_J over time.

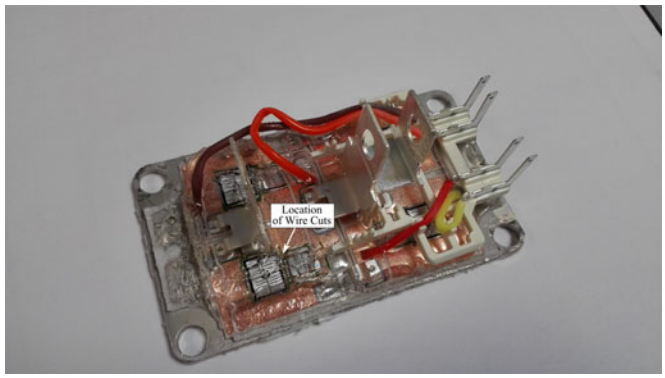

Fig. 19. Uncovered IGBT power module used for the wire-bond cut-off test.

Fig. 15 shows the probability density function (pdf) of the residual obtained at different numbers of cycles. It can be seen that as the number of cycles progresses the distribution of the residual shifts to the right, revealing a change in the mean value. Fig. 16 shows the mean value of the residual as function of number of cycles. Ideally, the value of the residual should start at zero, indicating a perfect match between the thermal model and the true thermal path. However, this is not the case because of errors in the modeling that result during the original identification of the thermal model. The residual mean follows a trend similar to the trend in R_{thja} shown in Fig. 3. After 11 300 cycles the residual shows a significant jump which is in good agreement with the observed increase in R_{thja} measured by the power cycling equipment. The small differences between the two curves can be justified by the measurement noise and disturbances acting on the module during normal operation, which can affect the residual as detailed earlier. It should be stressed that unlike the direct measurement of R_{thja}, which requires specific equipment and specific conditions, the residual is obtained during the normal operation of the power converter. This allows information about the extent of degradation in the thermal path to be obtained in the normal working environment of the power converter.

B. RLS Algorithm

The online measurement of current I_C and on-state voltage $V_{\mathrm{CE(ON)}}$ are used to estimate the electrical resistance R_{CE} using the RLS algorithm. Fig. 17 shows the convergence of the R_{CE} estimate to the true value of R_{CE}. The "true" value is determined offline from the forward characteristic as detailed earlier. It can be seen that the algorithm converges to the "true" value after about 75 iterations.

Fig. 18 shows the change in the online estimate of R_{CE} as the junction temperature T_J changes over time. In this case, the estimate of junction temperature T_J increases steadily in response to a gradual change in the cooling water temperature. A clear positive temperature coefficient of R_{CE} is visible in good agreement with the results of Fig. 9.

In order to evaluate the performance of the estimate of R_{CE} against wire-bond lift-off, the casing of one of the IGBT inverter modules was removed to allow access to the wire bonds and the wire bonds were manually cut, one by one. After each wire cut, the online data were collected and processed to estimate R_{CE}. Fig. 19 shows the uncovered IGBT module used for this test and the location of the wire bonds being cut.

Fig. 20 shows the estimated R_{CE} after each wire cut. The estimated value of R_{CE} at the original state, with eight intact wires, is about 5.49 mΩ but as the number of cut wires increases,

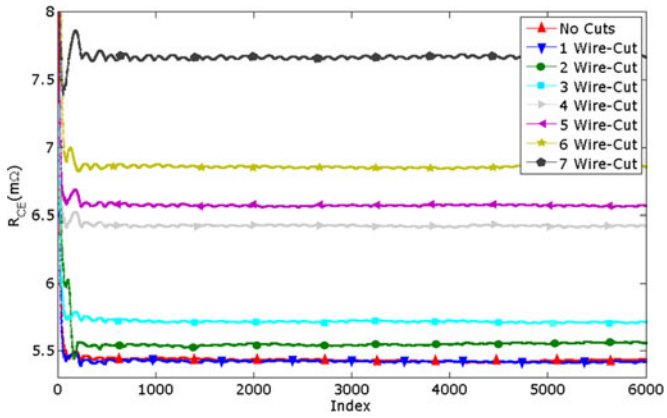

Fig. 20. Estimated R_{CE} after each wire cut. R_{CE} increases as the number of lost wires increases.

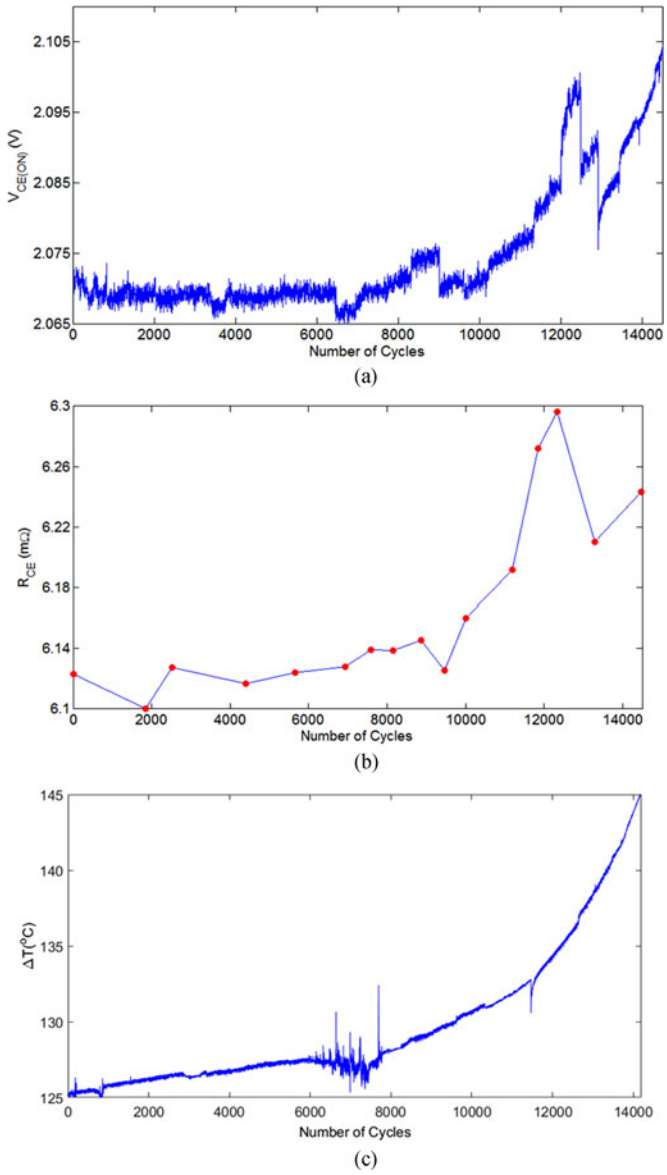

Fig. 21. (a) On-state voltage $V_{\mathrm{CE(ON)}}$ of the IGBT during the power cycling test. (b) R_{CE} estimated from the online measurements of $V_{\mathrm{CE(ON)}}$ and I_C using RLS during normal operation of inverter. (c) Junction temperature swing ΔT during the power cycling test.

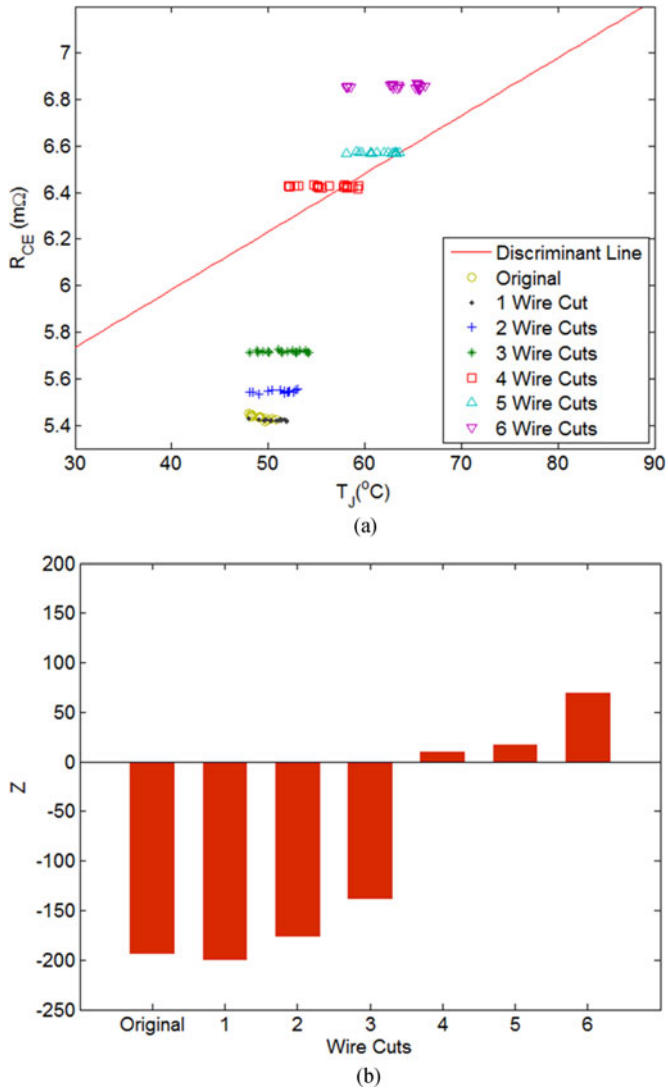

Fig. 22. (a) Discriminant line and the estimated data points (R_{CE}, T_J) as wires on the chip are cut. (b) Corresponding value of the linear transformation Z.

the estimated R_{CE} increases to reach 6.48 mΩ when four wires are cut and 7.7 mΩ when seven wires are cut.

Validation of the estimate of R_{CE} throughout the lifetime of IGBT was carried out as described in Section IV. The on-state voltage $V_{\mathrm{CE(ON)}}$ as a function of number of cycles is shown in Fig. 21(a). These data are measured by the power cycling equipment at a constant current value of 270 A and a temperature of 140 °C. Fig. 21(b) shows the estimate of R_{CE} given by the RLS algorithm from the online measurement obtained from the inverter during normal operation. There is clear correlation between the two parameters, where the changes in R_{CE} are consistent with the changes in $V_{\mathrm{CE(ON)}}$ during the power cycling test.

The step changes in the $V_{\mathrm{CE(ON)}}$ are assumed to be related to wire-bond lift-off (upward steps) and reattachment (downward steps). These latter downward steps are assumed to be caused when wires that have previously separated from the die surface re-make their electrical contact. In tandem with the step-changes in $V_{\mathrm{CE(ON)}}$ there is a gradual rise in $V_{\mathrm{CE(ON)}}$; this is related

to increases in junction temperature [see Fig. 21(c)] as a result of thermal degradation due to solder fatigue. Consequently, this method can be used to detect changes in R_{CE} caused either by variation of temperature or by wire-bond lift-off.

C. Discriminant Analysis

The discriminant line was arbitrarily designed to detect a change in R_{CE} of 15% from its original value. Fig. 22(a) shows the discriminant line and the data points of the estimated R_{CE} and its corresponding value of T_J obtained from the wire cutting test explained earlier. The spread in the data is due to measurement noise. It can be seen that as the wire bonds are lost the data shift up closer to the discriminant line until it crosses the line due to the increment in R_{CE}. It is also clear that T_J is increasing due to an increase in the die power dissipation. The linear transformation *Z* for this data is shown in Fig. 22(b). The value *Z* represents the normal distance of the data points (R_{CE}, T_J) from the discriminant line. Below the line the value of *Z* is negative. As the value of R_{CE} increases due to wire-bond failure, *Z* increases to become zero when R_{CE} reaches 15% above its original value and *Z* becomes positive when R_{CE} becomes higher than 15% of its original value. Importantly, if R_{CE} changes due to an increment in T_J, that change will be parallel to the discriminant line and therefore, the normal distance *Z* will not be affected. In this way, *Z* is only sensitive to changes in R_{CE} resulting from wire-bond failure.

VI. Conclusion

Degradation of power semiconductor packaging is a limiting factor adversely affecting the availability of power converters. Estimates of power semiconductor lifetime for applications with unpredictable mission profiles are prone to many uncertainties, making them unreliable as a tool for maintenance scheduling. Here a condition-monitoring approach is proposed to monitor the degradation of power semiconductor packages based on online measurements of operational parameters that can be obtained from the semiconductor (IGBT in this case) during its normal operation in the power converter. The two key degradation mechanisms of solder fatigue and wire-bond lift-off are related, respectively, to increases the thermal resistance R_{thja} and electrical resistance R_{CE} of the module.

This paper has presented two approaches to monitor, online, the degradation of IGBT modules: first, model-based residuals using a Kalman filter and second, parameter estimation using RLS. The online measurements of on-state voltage $V_{\mathrm{CE(ON)}}$, current I_C, and gate threshold voltage $V_{\mathrm{G(th)}}$ are made on the IGBT module. Gate threshold voltage $V_{(\mathrm{G})\mathrm{th}}$ is used by the Kalman filter to estimate junction temperature T_J whilst at the same time, generating a residual which is used to monitor the degradation of the thermal resistance R_{thja}. The on-state voltage $V_{\mathrm{CE(ON)}}$ and the current I_C are used by the RLS algorithm to estimate the electrical resistance R_{CE}. Since R_{CE} is sensitive to temperature variations, a linear transformation can be used to eliminate the influence of temperature on R_{CE} such that the linear transformation *Z* is sensitive only to changes in R_{CE}, in particular due to wire-bond failure. Experimental validation has shown that the proposed methods are capable of detecting changes in the module thermal path resistance R_{thja} and electrical resistance R_{CE} using measurements obtained at gate-drive level under normal converter operating conditions.

By combining the early indication of degradation with CBM, where degraded components are replaced before they fail destructively and unexpectedly, the presented condition monitoring approach can improve the availability of the assets utilizing power semiconductor packages such as wind turbines and electric trains.

References

[1] K. H. Michael Wilkinson and B. Hendriks, "Measuring wind turbine reliability: Results of the reliawind project," in *Proc. Eur. Wind Energy Conf.*, Brussels, 2011.

[2] Y. Shaoyong, A. Bryant, P. Mawby, X. Dawei, R. Li, and P. Tavner, "An industry-based survey of reliability in power electronic converters," *IEEE Trans. Ind. Appl.*, vol. 47, no. 3, pp. 1441–1451, May/Jun. 2001.

[3] X. Dawei, R. Li, P. Tavner, A. Bryant, Y. Shaoyong, and P. Mawby, "Monitoring solder fatigue in a power module using case-above-ambient temperature rise," *IEEE Trans. Ind. Appl.*, vol. 47, no. 6, 2578–2591, Nov./Dec. 2011. [Online]. Available: https://docs.wind-watch.org/Measuring_Wind_Turbine_Reliability_-_Reliawind.pdf

[4] X. Dawei, L. Ran, P. Tavner, Y. Shaoyong, A. Bryant, and P. Mawby, "Condition monitoring power module solder fatigue using inverter harmonic identification," *IEEE Trans. Power Electron.*, vol. 27, no. 1, pp. 235–247, Jan. 2012.

[5] J. M. Anderson and R. W. Cox, "On-line condition monitoring for MOSFET and IGBT switches in digitally controlled drives," in *Proc. 2011 IEEE Energy Convers. Congr. Expo.*, 2011, pp. 3920–3927.

[6] J. Lehmann, M. Netzel, R. Herzer, and S. Pawel, "Method for electrical detection of bond wire lift-off for power semiconductors," in *Proc. IEEE 15th Int. Symp. Power Semicond. Devices*, 2003, pp. 333–336.

[7] S. Yang, D. Xiang, A. Bryant, P. Mawby, L. Ran, and P. Tavner, "Condition monitoring for device reliability in power electronic converters: A review," *IEEE Trans. Power Electron.*, vol. 25, no. 11, pp. 2734–2752, Nov. 2010.

[8] V. K. Sundaramoorthy, E. Bianda, R. Bloch, and F. Zurfluh, "Simultaneous online estimation of junction temperature and current of IGBTs using emitter-auxiliary emitter parasitic inductance," in *Proc. PCIM Eur. 2014*, 2014, pp. 1–8.

[9] V. Sundaramoorthy, E. Bianda, R. Bloch, I. Nistor, G. Knapp, and A. Heinemann, "Online estimation of IGBT junction temperature (Tj) using gate-emitter voltage (Vge) at turn-off," in *Proc. 15th Eur. Conf. Power Electron. Appl.*, 2013, pp. 1–10.

[10] I. Č. Bahun, C. Neven, and Z. Jakopović, "Real-time measurement of IGBTs operating temperature," *Automatika: J. Control, Meas., Electron.*, vol. 52, pp. 295–305, 2011.

[11] P. Ghimire, K. B. Pedersen, A. R. D. Vega, B. Rannestad, S. Munk-Nielsen, and P. B. Thogersen, "A real time measurement of junction temperature variation in high power IGBT modules for wind power converter application," in *Proc. 8th Int. Conf. Integr. Power Syst.*, 2014, pp. 1–6.

[12] MentorGraphics, Power Tester 1500A. [Online]. Available: https://www.mentor.com/products/mechanical/micred/power-tester-1500a/

[13] M. A. Eleffendi, L. Yang, P. Agyakwa, and C. M. Johnson, "Quantification of cracked area in thermal path of high-power multi-chip modules using transient thermal impedance measurement," *Microelectron. Rel.*, vol. 59, pp. 73–83, 2016.

[14] Infineon Application Note ANIP9931E "Calculation of major IGBT operating parameters," Infineon Technologies, 1999. [Online]. Available: http://www.infineon.com.

[15] K. B. Pedersen, P. K. Kristensen, V. Popok, and K. Pedersen, "Degradation assessment in IGBT modules using four-point probing approach," *IEEE Trans. Power Electron.*, vol. 30, no. 5, pp. 2405–2412, May 2015.

[16] J. R. Celaya, A. Saxena, S. Saha, and K. Goebel, "Prognostics of power MOSFETs under thermal stress accelerated aging using data-driven and model-based methodologies," in *Proc. Annu. Conf. Prognostics Health Manage. Soc.*, vol. 2, 2011, pp. 1–10.

[17] A. Eleffendi and C. M. Johnson, "Application of Kalman filter to estimate junction temperature in IGBT power modules," *IEEE Trans. Power Electron.*, vol. 31, no. 2, pp. 1576–1587, Feb. 2016.

[18] J. Gertler, "Analytical redundancy methods in fault detection and isolation," in *Proc. IFAC Symp. Fault Detection Supervision Safety Tech. Process.*, 1991, pp. 9–21.
[19] A. Eleffendi and C. M. Johnson, "Evaluation of on-state voltage VCE(ON) and threshold voltage Vth for real-time health monitoring of IGBT power modules," in *Proc. 17th Eur. Conf. Power Electron. Appl.*, 2015, pp. 1–10.

Mohd. Amir Eleffendi received the B.Sc. degree in computer engineering from the University of Aleppo, Aleppo, Syria, in 2009, the M.Sc. degree in control systems from the University of Sheffield, Sheffield, U.K., in 2011, and the Ph.D. degree in electrical and electronics engineering from the University of Nottingham, Nottingham, U.K., in 2016.

His research interests include prognostics and health management for power electronics and power semiconductors, fault detection and diagnosis algorithms, thermo-sensitive electrical parameters, active gate drives and thermal management.

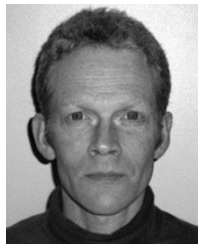

C. Mark Johnson (M'90) received the B.A. degree in engineering and the Ph.D. degree in electrical engineering from the University of Cambridge, Cambridge, U.K., in 1986 and 1991, respectively.

From 1990 to 1992, he was a Research Associate at the University of Cambridge, and in 1992, he joined as a Lecturer the University of Newcastle, Callaghan, U.K., where his research included the design, analysis, and characterization of power semiconductor devices, resonant power conversion, and instrumentation. From 1998 to 2001, he managed the U.K. national program on Silicon Carbide electronics, and in 2000, he became a Reader of power electronics at the University of Newcastle. In 2003, he was appointed as the Rolls-Royce/RAEng Research Professor of power electronic systems at the University of Sheffield, and in 2006, he was appointed to a personal chair at the University of Nottingham, where he leads research into power semiconductor devices, power device packaging, reliability, thermal management, power module technologies, and power electronic applications. He is the Director of the U.K. Engineering and Physical Sciences Research Council Centre for Power Electronics, which combines the UK's best academic talent to address the key research challenges underpinning power electronics, and is a member of the Executive for the U.K. Innovative Electronics Manufacturing Research Centre, Loughborough, U.K.